ISTITUTO NAZIONALE DI RICERCA METROLOGICA
Repository Istituzionale

Water-Mediated Ionic Migration in Memristive Nanowires with a Tunable Resistive Switching Mechanism

(Article begins on next page)

29 July 2022

Water-mediated ionic migration in memristive nanowires with tunable resistive switching mechanism

Gianluca Milano[1,2‡], Federico Raffone[1‡], Michael Luebben[3,4], Luca Boarino[2], Giancarlo Cicero[1], Ilia Valov[4,5]*, Carlo Ricciardi[1]*

[1]Department of Applied Science and Technology, Politecnico di Torino, C.so Duca degli Abruzzi 24, 10129 Torino, Italy.

[2]Advanced Materials Metrology and Life Science Division, INRiM (Istituto Nazionale di Ricerca Metrologica), Strada delle Cacce 91, 10135 Torino, Italy.

[3]Institute for Materials in Electrical Engineering II, RWTH Aachen University, Sommerfeldstrasse 24, 52074 Aachen, Germany.

[4]JARA – Fundamentals for Future Information Technology, 52425 Jülich, Germany.

[5]Peter-Grünberg-Institut (PGI 7), Forschungszentrum Jülich, Wilhelm-Johnen-Straße, 52425 Jülich, Germany.

ABSTRACT

Memristive devices based on electrochemical resistive switching effects have been proposed as promising candidates for in-memory computing and for the realization of artificial neural networks. Despite great efforts for understanding nanoionic processes underlaying resistive switching phenomena, the comprehension of the effect of competing redox processes on device functionalities from materials perspective still represents a challenge. In this work, we experimentally and theoretically investigate the concurring reactions of silver and moisture and their impact on the electronic properties of a single crystalline ZnO nanowire (NW). A decrease in electronic conductivity due to surface adsorption of moisture is observed, whereas in same time water molecules reduce the energy barrier for Ag^+ ion migration on the NW surface, facilitating the conductive filament formation. By controlling the relative humidity, the ratio between intrinsic electronic conductivity and surface ionic conductivity can be tuned to modulate the device performance. The results achieved on a single crystalline memristive model system shed new light on the dual nature of the mechanism how moisture affects resistive switching behavior in memristive devices.

INTRODUCTION

Memristive devices based on nanoionic redox processes are considered one of the most promising candidates not only for the realization of next-generation memories, but also for the emulation of brain functionalities through the implementation of neuromorphic-type data processing.[1–7] Despite recent breakthroughs in the implementation of neuromorphic algorithms in large memristive networks,[8–12] a detailed understanding of the complex redox behaviour and of the ionic processes at the single device level still represents a challenge. Redox-based memristors are two terminal devices in which the functionalities are enclosed in the resistive switching properties of a solid electrolyte, usually a metal-oxide film, sandwiched in between two metal electrodes.[13–17] In the established literature, the switching mechanism is related to nanoionic processes of migration of oxygen species (valence change memory effect, VCM) or host metal ions from an electrochemically active electrode (electrochemical metallization memory effect, ECM) or both of them.[18] Although the great efforts in investigating the switching mechanism, the role of extrinsic effects such as the surrounding environment on the memristive behaviour still needs to be elucidated. In particular, the influence of moisture on resistive switching has raised as one of the most important open issues related to the comprehension and control of resistive switching events.[19] Moisture incorporated from the surrounding environment or during device fabrication was reported to significantly influence the resistive switching properties of devices, representing concurring, but also essential nanoionic processes for proper operation of memristive cells.[20,21,30,22–29] However, no works consider the primer influence of adsorbed or absorbed moisture on the intrinsic electronic properties in memristive devices. Amorphous or polycrystalline films often have variable physicochemical properties such as structure, chemical

3

composition and stoichiometry which can vary during switching operations. These materials can also dissolve and/or incorporate ions and/or atoms and even clusters during operations and a different distribution of active places/centers can be expected. Density and nanoporosity of a given material can vary depending on the deposition conditions resulting in a different ability to incorporate water molecules.[31] Moreover, in metal-oxide thin films ambient moisture as a parallel and concurring redox reaction and a source of different ionic species can suppress or enhance the coexistence of VCM and ECM mechanisms.[32] From technical point of view, the vertical device structure does not allow to precisely define high quality interface between oxide and moisture where the processes could be clearly observed and studied. In this context, devices based on nanostructures with high surface-to-volume ratio have been proposed as an essential step for investigating the role of the surrounding environment on resistive switching phenomena.[33–35] However, no suitable model system has been proposed up to date.

In this work, we experimentally and theoretically investigate the interplay and dual influence of moisture on resistive switching properties of a monocrystalline ZnO nanowire (NW) as memristive model system. The individual NWs are contacted by means of asymmetric Ag and Pt electrodes to form an electrochemical metallization memory (ECM) cell with planar structure.[4] Both adsorption of water molecules from the surrounding environment as well as ionic migration are spatially restricted on the NW surface, making these devices an ideal (nano)platform for the investigation of the role of ambient on the physical mechanism of switching. Moisture absorbed on the NW surfaces, modifies the NW band structure and decreases its electronic conductivity. In addition, adsorbed water molecules not only reduce the electroforming voltage but also facilitate subsequent switching cycles. According to *ab initio* Density Functional Theory (DFT)

calculations, this influence can be interpreted in terms of reduction of the energy barrier for ionic migration of Ag^+ species on the crystalline NW surface in presence of adsorbed water molecules. Using dry environment results in unreliable and stochastic switching characteristics, if forming was possible at all.

EXPERIMENTAL METHODS

NW synthesis

ZnO NWs were realized by means of Low Pressure Chemical Vapor Deposition (LP-CVD) in a quartz horizontal tubular furnace, following the procedure previously reported.[36,37] In brief, a Pt thin film used as a catalyst was placed in the quartz tube on an alumina boat surrounded by a Zn foil (purity 99.99 %) that was used as Zn source. The CVD process was performed at 650°C for 20 min by flushing 300 sccm of Ar as carrier gas and 200 sccm of O_2 as gas precursor at a pressure of 1.6 Torr. As a result of this growth process along the [0001] direction, an high density array of vertically aligned and hexagonal shaped ZnO NWs was obtained on the Pt substrate. A cross-sectional SEM image of as grown ZnO NWs is reported in Supplementary Information S1.

Device fabrication

Single NW memristive devices were realized by means of a combination between optical and electron beam lithography (EBL), as previously reported.[4,38] Initially, ZnO NWs were mechanically transferred from the growth substrate onto a SiO_2 insulating substrate that was pre-patterned with a probe circuit realized by optical lithography and Cr/Au deposition. Contact geometries to contact single isolated nanostructures with the probe circuit were realized by means of EBL (FEI Quanta™ 3D Microscope) and subsequent metal deposition (thickness of 80 nm). In order to realize asymmetrically contacted NWs with Pt and Ag electrodes, two subsequent EBL

processes were performed. During all these fabrication steps, ZnO NWs were not exposed to aqueous solutions in order to avoid corrosion of the surface.[39]

Atmosphere-controlled electrical characterization

Atmosphere-controlled electrical characterizations were performed in a customized probe station.[23] The probe station is equipped with a chamber in which the atmosphere can be modified in terms of gas composition. Measurements were performed in air, N_2 environment (dry) and at different levels of moisturized N_2. Measurements at different moisture levels were performed in an N_2 environment by fluxing N_2 through a cascade of gas wash bottles filled with deionized water. The relative humidity in the chamber was measured by means of an analog humidity sensor. Before atmosphere-controlled measurement, the chamber is evacuated down to $\sim 10^{-5}$ mbar and then refilled with the desired gas compositions. Electrical measurements were performed after stabilization of the ambient conditions by using a Keithley 2636A or a Keithley 2636B. In all measurements, the Pt electrode of the memristive cell was grounded while the Ag electrode was positively biased. During the electroforming process and subsequent resistive switching cycles, a compliance current of 10 μA was applied in order to prevent the full breakdown of the device. All electrical measurements were performed at room temperature.

Density Functional Theory method

The computational analyses were performed within the Density Functional Theory framework using the QUANTUM ESPESSO package.[40] The Perdew–Burke–Eenzerhof (PBE)[41] formulation of the general gradient approximation was used to approximate the exchange-correlation potential while electron−ion interaction was described with ultrasoft pseudopotentials.[42] A plane wave basis set with 28 Ry cutoff was employed to model the wave functions and a 280 Ry cutoff to model the

6

density. The ZnO NW was reproduced simulating the exposed (1$\underline{1}$00) surface (that is the lateral surface of the NW) represented by 12 layers ZnO slabs with 2 × 2 surface supercell and periodic boundary conditions. The supercell included a 15 Å vacuum layer in the direction perpendicular to the surface to avoid spurious interactions among replicas. The Brillouin Zone was sampled with a (3 × 3 × 1) Monkhorst-Pack k-point grid. The potential energy surface analysis (PES) was obtained by placing a Ag adatom at 15 evenly spaced positions in the irreducible part of the (2 × 2) surface cell at an initial distance from the surface atoms of 2.5 Å. The Ag atoms were allowed to relax in the direction perpendicular to the surface only (z) until forces were smaller than 26 meV/Å.

RESULTS AND DISCUSSION

Influence of moisture on electronic conduction

The synthesis of ZnO NWs was performed by LP-CVD (details in experimental methods section), resulting in vertically aligned NWs as reported in Figure 1a. The median length and diameter of NWs are measured to be ∼1.6 µm and ∼ 100 nm (aspect ratio of ∼16) from the analysis of cross-sectional SEM images (Supplementary Information S1). The hexagonal ZnO NWs have wurtzite crystal structure with P6$_{3mc}$ symmetry and the growth process proceeds along the [0001] polar direction,[37] as shown in Figure 1b. A detailed structural and chemical characterization of ZnO NWs revealed that each NW is a monocrystal characterized by high chemical purity and a clean surface (no amorphous layers were observed on the NW surface), as investigated in our previous works.[37,39] Single ZnO NWs dispersed on an insulating SiO_2 substrate and contacted by means of asymmetrical Pt and Ag contacts were exploited as memristive model systems to investigate the

7

influence of moisture on resistive switching mechanism by means of atmosphere-controlled measurements, as schematized in Figure 1c. Device fabrication and experimental setup exploited for atmosphere-controlled measurements is discussed in the experimental methods section. It is worth noticing that, since the NW growth proceeds along the [0001] polar direction, surfaces exposed to the surrounding environment in single NW memristive devices are the non-polar (1-100).

Ag/ZnO NW/Pt devices can be considered as electrochemical metallization memory cells where device functionalities are regulated by ionic processes that are coupled to the electronic ones.[4,43] In the pristine state, electronic conduction mechanism is governed by Schottky barriers formed at the Pt/ZnO and Ag/ZnO interfaces and the device can be electrically described by means of two back-to-back connected Schottky diodes with the NW series resistance.[44] In this context, *I-V* characterizations revealed that electronic conduction of the device is regulated by adsorbed species on the ZnO NW surface (Supplementary Information S2). Among adsorbed species, water molecules play a key role in determining the formation of a depletion region with upward band bending on the NW surface, while no diffusion of water molecules in the crystalline ZnO bulk structure was reported.[45] Depending on the moisture level, the amount of adsorbed water molecules on the NW surface regulates the extent of the depleted shell layer, resulting in a change of the effective diameter of the NW inner core that actively participates in the electronic conduction (a band diagram schematization is reported in Supplementary Information S2). Therefore, an increase of the moisture level is responsible for an increase of the NW resistance. Also, our observations suggested that water electrolysis occurring when the device is biased can influence the electronic conduction mechanism of ZnO NWs, being responsible for an increase of resistance due to the

8

creation of OH groups that can be consequently attached on the nonpolar lateral surfaces of the NW (details in Supplementary Information S3).

Influence of moisture on ionic conduction

Despite influencing the electronic conduction mechanism, moisture can strongly influence also ionic conduction properties underlying memristive behaviour of single crystalline ZnO NWs. In these devices, memristive functionalities are driven by the electrochemical metallization memory effect that involves dissolution of the electrochemically active electrode (Ag) and migration of metal ions along the NW surface under the action of the applied electric field to form a conductive path in between the electrodes.[4,46–49] It is worth noticing that the coexistence of ECM and VCM mechanisms of switching can be safely excluded in these devices as a consequence of the high ZnO crystal quality.[4] The initial assessment of the metallic path in between the electrodes can be performed by means of the so-called electroforming process, by applying a positive voltage sweep to the electrochemically active Ag electrode. The *I-V* characteristics of a typical electroforming process performed in ambient air is shown in Figure 1d. In the low voltage range (1.), the device exhibited the characteristic of a forward biased diode. By further increasing the voltage bias (2.), a current saturation regime was observed. This results from the Pt/ZnO junction that, while it appears as an ohmic contact in the low voltage range, acts as a reversely polarized Schottky barrier for high applied voltages.[4] Then, the device turns from a high resistance state (HRS) to a low resistance state (LRS) in correspondence of the forming voltage where an abrupt current jump can be observed due to the formation of an Ag conductive path along the NW (3.). Our results revealed that the electroforming process is strongly influenced by the moisture level in the surrounding

environment. In a first experiment, voltage sweeps were applied to a single NW memristive cell with electrode spacing of 376 nm by progressively increasing the amount of moisture in a N_2 environment. While the formation of a conductive path was not possible in case of dry N_2 and relative humidity (RH) of 47%, a current jump testifying a successful electroforming was observed when the humidity content was increased to RH = 71% (Supplementary Information S4). In a second experiment, three different NW memristive cells with same electrode spacing (~ 150 nm) were electroformed at different moisture levels. Results reported in Figure 1e revealed that devices measured at higher moisture level exhibited a severe reduction of the forming voltage. Indeed, the forming voltage decreased from about 11.6 V to 9.4 V and 6.6 V passing from dry N_2 to RH = 48 % and RH = 71 %, respectively. Last, the forming voltage measured in dry N_2 or at RH = 70% as a function of electrode spacing for different single NW devices is reported in Figure 1f. Besides an expected decrease of the forming voltage by decreasing the electrode spacing, a substantial reduction of the forming voltage was observed for devices electroformed at RH = 70 %. All these results unequivocally show that moisture strongly influences the electroforming process, evidencing a substantial reduction of the forming voltage by increasing the moisture level in the surrounding environment. It is worth noticing also that all electroforming processes were performed by applying a voltage sweep rate of 0.7 V/s, since the voltage sweep rate applied to the NW device was observed to strongly influence the forming voltage, as discussed in our previous work.[4] In summary, the electroforming voltage can be modified and engineered by: *i)* tuning the electric field in between electrodes by adjusting the electrode spacing, *ii)* regulating the device kinetics by regulating the voltage sweep rate of stimulation, and *iii)* by tuning the ionic conduction mechanism by adjusting the level of moisture as discussed in the following.
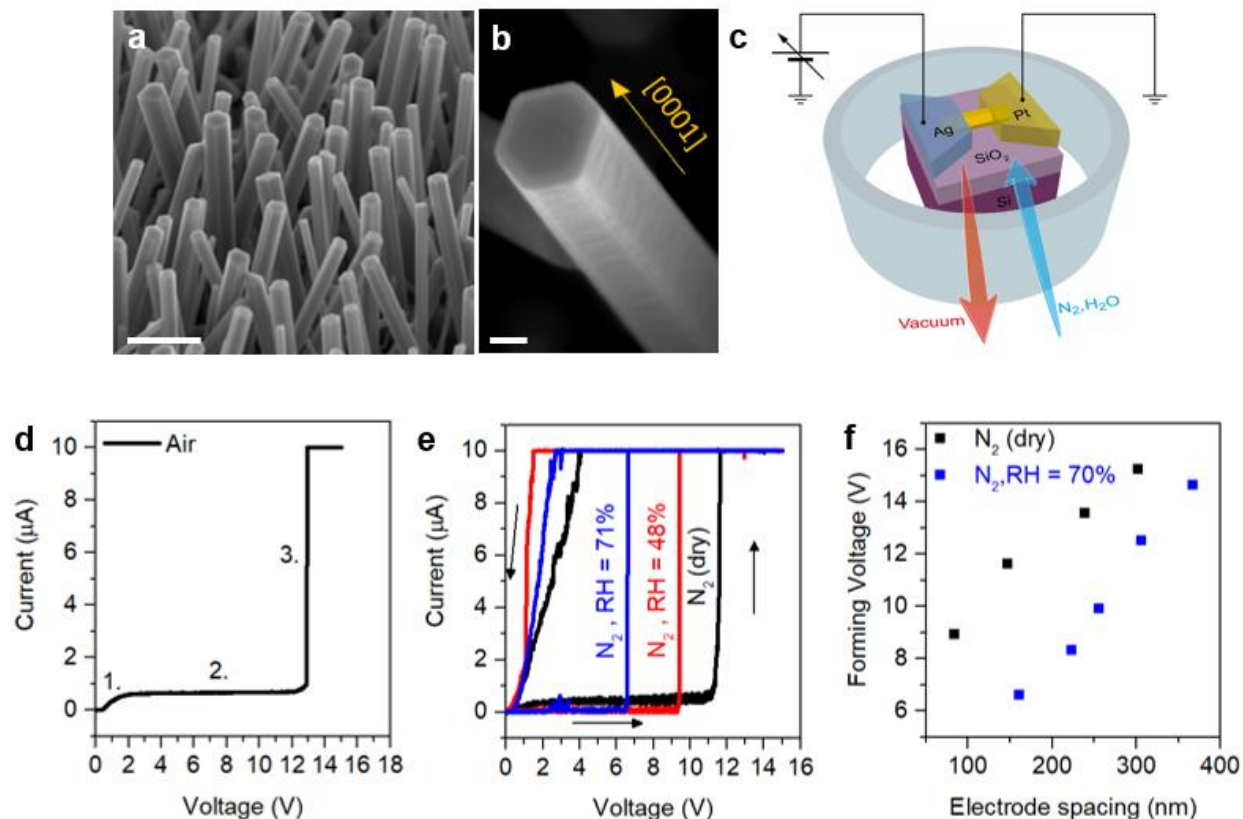
10

Figure. 1. ZnO NW based memristive device and influence of moisture on electroforming. (a) SEM image of NW arrays after the growth process (scale bar, 500 nm) and (b) detail of a single ZnO NW with hexagonal shape grown along the [0001] polar direction (scale bar, 40 nm) (c) Schematic representation of a single NW based memristive device with electrical connections in an atmosphere-controlled chamber. (d) Typical electroforming process of a single NW memristive cell in air, evidencing a diode-like behaviour for V < 1.5V (1.), current saturation regime for higher voltages (2.) and an abrupt change in resistance due to the formation of an Ag conductive path (3.). (e) Comparison of the electroforming curves of NW memristive cells with same electrode spacing (~ 150 nm) in N_2 environment at different levels of moisture showing a reduction of the forming

voltage in devices electroformed at higher levels of RH. (f) Electroforming voltage as a function of electrode spacing for different devices electroformed in N_2 environment in dry conditions and at RH = 70 %, revealing a substantial reduction of the forming voltage in devices electroformed in presence of moisture. Electrical measurements were performed at room temperature.

Influence of moisture on resistive switching behavior

Electroforming represents the ideal process for investigating the influence of moisture on the ionic transport mechanism since the device is initially in the pristine state and no metallic clusters are present on the NW surface. This means that ionic migration has to proceed along all the electrode spacing before observing a change in the device resistance. However, it is shown here that also subsequent resistive switching cycles, involving the formation/rupture of a metallic path due to the migration of Ag^+ ions in between nanoclusters that are present on the NW surface after electroforming, is also affected by the moisture level. After electroforming, the device measured in air exhibited stable bipolar resistive switching characterized by an HRS/LRS ratio > 200, as reported in Fig. 2(a) and (b), respectively. Endurance and retention characteristics of single ZnO NW-based memristive devices in air are reported in our previous work.[4] After 25 cycles in air, the chamber was evacuated and then filled with N_2. Under dry conditions, the device did not exhibit resistive switching since no SET events were recorded after device stimulation with repeated voltage sweeps as reported in Fig. 2(c). This means that resistive switching is suppressed in absence of moisture, at least by considering the same range of applied voltage. In addition, suppression of resistive switching was directly observed in real time by reducing the moisture content in the surrounding environment over cycling (Supplementary Information S5). It is worth

noticing that the resistive switching behaviour suppressed in dry conditions can be restored by exposing the device again to humidity (Supplementary Information S6). All these results reveal that ionic dynamics underlying resistive switching behaviour are strongly influenced by moisture.
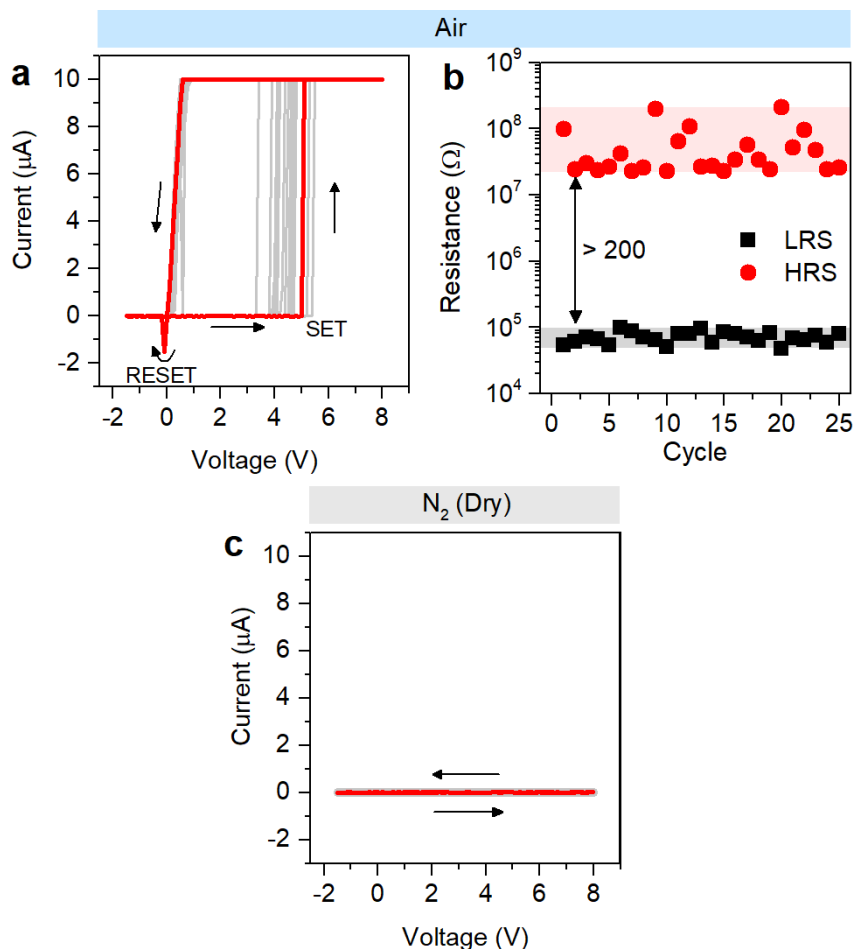

Figure 2. Influence of moisture on resistive switching behaviour. (a) I-V characteristics showing bipolar resistive switching behaviour of a single ZnO NW in air (RH ≈ 30 %) and (b) corresponding HRS and LRS values over cycling extrapolated at a reading voltage of 0.4 V. (c) I-V characteristics of the same device in dry air (N$_2$ environment) showing suppression of the resistive switching behaviour. In both cases, the device was stimulated by means of 25 DC voltage

sweeps in the voltage range -1.5/8 V. Electrical measurements were performed at room temperature.

Morphological changes of the device after switching events

Due to the planar structure of the single NW memristive device and to the restriction of ionic migration on the crystalline surface, ionic transport properties can be directly investigated by analyzing the morphology of the conductive path after resistive switching. While the pristine device exhibited a clean surface (Fig. 3(a)), nanoclusters were observed on the ZnO crystalline surface after resistive switching events (Fig. 3b). In particular, a high resolution SEM image acquired with secondary electrons (SE) revealed details on the nanoclusters size and distribution (Fig. 3c), while imaging with backscattered electrons (BSE) was used to provide information on the nanocluster composition (Fig. 3d). Being BSE imaging highly sensitive to differences in atomic number making possible a differentiation of metals based on contrast, it can be observed that the brilliance of nanoclusters is comparable to the brilliance of the Ag electrode, confirming that these nanoclusters are made of Ag. Note that these observations are in accordance with previous TEM and EDS analysis,[4] corroborating the previously discussed switching mechanism. Interestingly, Ag nanoclusters were observed to be mainly accumulated near the Ag electrode suggesting a conductive filament growth from the electrochemically active electrode towards the inert counter electrode. This filament growth dynamics are typical of memristive systems characterized by low cation mobility, where Ag^+ ions transport represents a rate limiting process for the conductive path formation.[50,51] Moreover, it is important to point out that the interaction of water molecules with the ZnO surface can be responsible for corrosion of the crystalline oxide.[39,52] However, while ZnO

14

NWs after prolonged immersion in liquid water exhibited a wrinkled and corroded surface (Supplementary Information S7), no significant corrosion effects were observed by exposing ZnO NWs to moisture and the smooth surface was preserved.
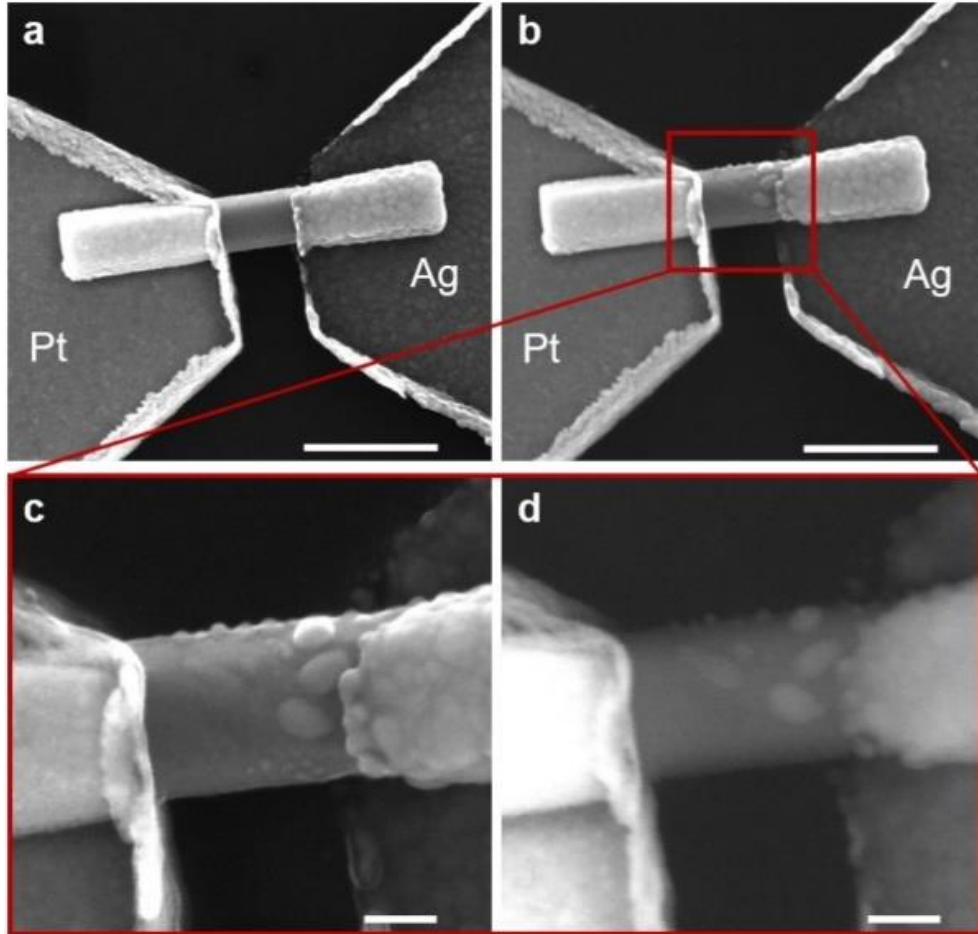

Figure. 3. Change of device morphology after resistive switching. Scanning Electron Microscopy (SEM) image of (a) a single ZnO NW memristive device in the pristine state and (b) the same device after resistive switching (scale bars, 500 nm). Enlarged view of the device after resistive switching acquired with (c) secondary electrons and (d) backscattered electrons showing the presence of Ag nanoclusters on the ZnO crystalline surface accumulated mainly near the

electrochemical active Ag electrode as a consequence of the low cation mobility (scale bars, 100 nm).

Density Functional Theory (DFT) simulations

In the following, we provide an atomistic characterization of the drift process of Ag atoms on top of ZnO crystalline NW by means of Density Fuctional Theory (DFT) simulations with the objective of understanding whether the presence of moisture molecules on the NW surface affects the silver rate of diffusion. The details of the simulations are provided in the methods section. We simulated the crystalline nanowire surface in two conditions: bare (Fig. 4a and b)) and with 1 monolayer (ML) of water (Fig. 4(c,d)) adsorbed, as representative, respectively, of the dry and high humidity conditions. A high water pressure is, indeed, likely to cause the water molecules to adsorbe at the NW surface. According to our calculations, the molecules attach on the Zn atoms belonging to the topmost surface layer (see Figure 4c and 4d), in agreement with previous studies on ZnO surfaces.[53] One of the two hydrogen atoms of water forms a hydrogen bond with the NW oxygen surface atom while the other is H-bonded to nearby H_2O molecule. Intermediate humidity stages will be likely characterized by bare and covered patches of different sizes. The different degree of humidity will determine in general the amount of adsorbed water on the surface.

For both bare and water covered surfaces, we performed a PES for the adsorption of a single silver atom on the NW (1-100) non-polar lateral surfaces. The PES reveals the presence of diffusion barriers for Ag atom along the NW axes and allows quantifying how likely the diffusion process is to occur as previous studies have shown.[49,54] In the bare surface case, an analysis of Figure 4b shows that for the diffusion of Ag atoms in the growth direction of the NW [0001], two barriers

16

must be overcome: a smaller one (0.03-0.17 eV depending on the direction of motion) and a larger one (0.64-0.78 eV). Notably, the largest one is located by the topmost Zn surface atoms which interacts repulsively with Ag, being both metal species positively charged. The barrier represents the rate limiting step of the drift process in vacuum. A representation of the diffusion path along the [0001] direction on the bare surface is shown in the Figure 5a-e where it is possible to see the Ag atom moving on top of the ZnO surface. From the most stable position (Figure 5a) located within a ZnO surface ring, the silver atom moves toward the Zn highest row (b-c) which, as said, constitutes the primary obstacle for the diffusion. In the following steps (d-e) the adatom moves on top of uppermost lying Zn-O dimer in order to reach the next ZnO ring. In these positions the energy is lowered by the interaction with the surface oxygen atom. Concerning the perpendicular [11$\underline{2}$0] direction, there is no barrier preventing the lateral motion of silver atoms.

When the surface is covered by water, the diffusion mechanism changes drastically as indicated by the altered PES. Unlike the bare case where the barriers are quite flat in the [11$\underline{2}$0] direction, the PES profile is highly uneven as consequence of the adsorbed H_2O molecules orientation. As it can be seen in Figure 4d, when the Ag atoms are on the left side of a water molecule, the PES is particularly flat. This result can be understood by looking at the Ag as it moves in the [0001] direction (in Figure 5f-j). The metal atom almost never closely interacts directly with the surface, but it rather travels on top of the adsorbed water molecules. A bond is formed between the silver atom and water molecules which, in turn, split into OH^- and H^+. An Ag-OH complex, bound to the surface, is formed while the remaining H^+ attaches to one of the oxygens of the ZnO NW surface (compare Figure 5g and h). Because of the presence of the water molecules, when drifting in the electric field direction ([0001]), the silver atom avoids the repulsive interaction with the outmost

Zn layer (Figure 5i) and, thus, the energy profile is rather flat as seen in Figure 4d. The limiting barrier is only 0.33 eV; the highest energy configuration corresponds to a highly stretched Ag-OH complex (see Figure 5g). If, instead, the silver atom moves on the right side of the adsorbed water molecules, the complex cannot be formed so the PES presents much higher energy maxima.

The moisture has, therefore, a crucial effect on the switching process of ReRAM devices enabling their operations thanks to the aiding effect of the water molecules covering the NW surface. A drastic change in the diffusion mechanism is observed. In absence of moisture, surface Zn atoms suppress the movement of the adsorbed Ag atoms hampering ionic dynamics responsible for resistive switching. In contrast, when the humidity, and thus the surface coverage with water molecules, is high enough to ensure a percolation path where the Ag atoms can readily travel on top of the adsorbed water molecules avoiding the repulsive Ag-Zn interaction, the device is easily formed, as the diffusion barrier will be significantly lowered by the presence of water molecules. Moreover, it should be pointed out that the here proposed water-mediated ionic migration mechanism with enhanced diffusion of Ag^+ in a humid medium holds also in presence of dissociated water or hydroxyl groups on the ZnO surface resulting from water electrolysis. Indeed, the major effect of the adsorbed water is to avoid the repulsive interaction between the moving Ag atom and the topmost Zn atom. This is achieved by dissociation of water into $OH^\bullet + H^\bullet$ (where $^\bullet$ indicates a bond with the surface). The $OH^\bullet$ dangling bond is saturated by the Ag atom moving in the direction of the electric field ([0001]). As the OH group is located exactly between the Ag and the topmost Zn, the repulsive interaction between them is negated. Because the single $H^\bullet$ adsorbed on the surface plays no role, we can assume that the same mechanism holds for a surface covered with only OH groups. Based on these results, electrolysis is suggested not to influence ionic

conduction mechanism even if it is not possible to exclude that this effect can be involved in regulating the memristive cell electrochemistry participating in the counter electrode reaction as reported in thin-film based devices,[19,21,23] even if in our case we did not observed any bubbles or deformation of metallic electrodes related to electrolysis phenomena. Last, it should be remarked that moisture is expected to support corrosion of the Ag conductive path after its formation (i.e. in the ON state), leading to an expected poorer retention characteristic of the device.[19]
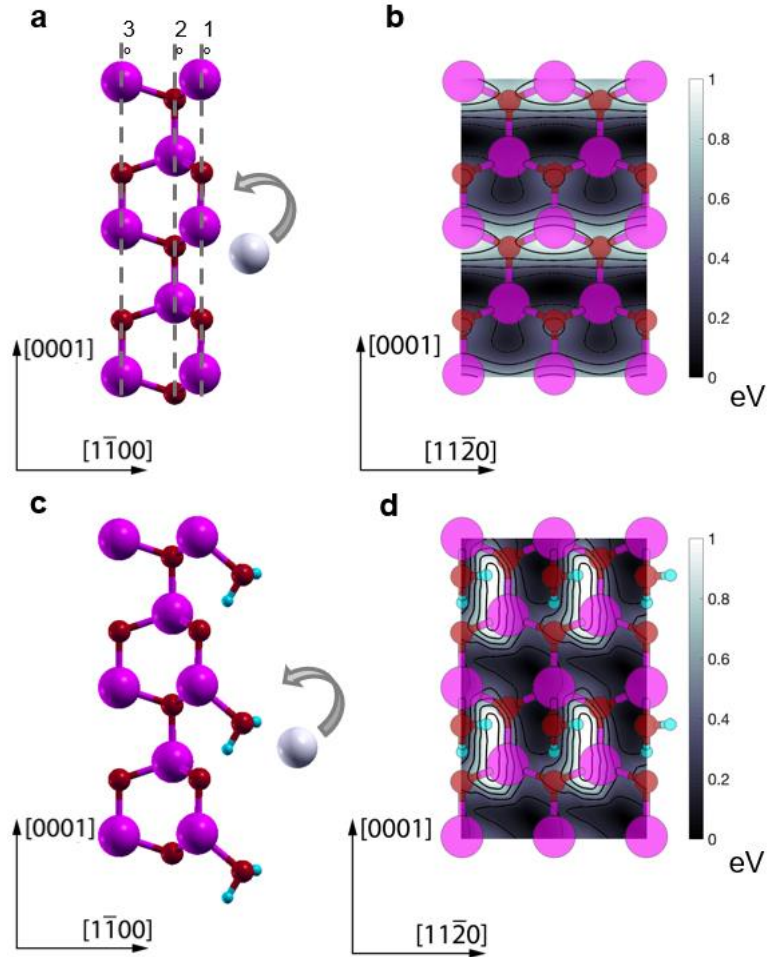
Figure 4. Theoretical investigation of the effect of adsorbed water on electric field assisted Ag ions migration. Left side: ball and stick representation of a silver atom adsorbed on the ZnO NW bare (1-100) surface (a) and on the ZnO NW (1-100) surface with 1 ML of adsorbed water molecules (c) in a side view. Zinc, oxygen, hydrogen and silver atoms are represented respectively in magenta, red, cyan and gray. In panel (a), 1°, 2° and 3° dashed line indicate the position of, respectively, the topmost, second highest and third highest ZnO layers, respectively. Right side: top view and related potential energy surface for the adsorption of a silver atom on top of a bare ZnO (1-100) surface (b) and on the water covered ZnO (1-100) surface (d) where the color bar was

truncated to 1 eV and the zero energy was set to the lowest adsorption energy. Contour lines are plotted every 0.2 eV step.
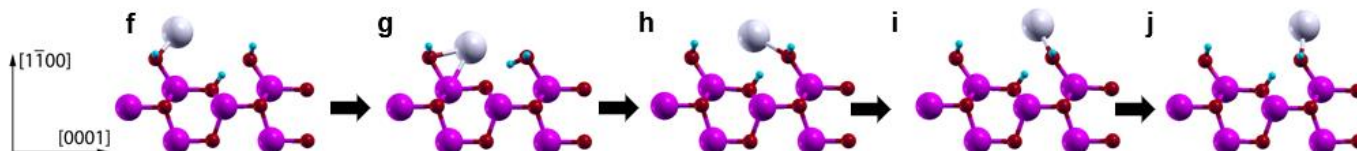

ZnO bare surface
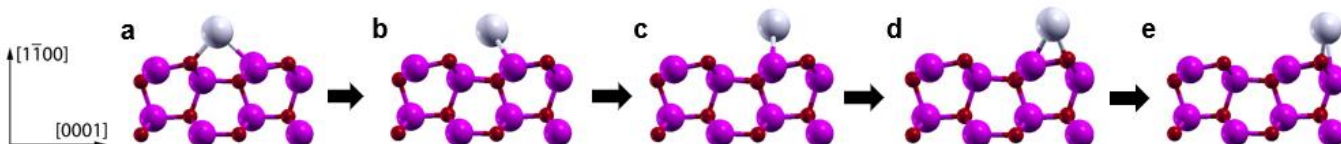
H₂O-covered ZnO surface

Figure. 5 Ball and stick representations of the diffusion mechanism of an Ag atom at the bare (a-e) and H$_2$O covered (f-j) ZnO(1$\underline{1}$00) surface in the [0001] direction (side view). Zinc, oxygen, hydrogen and silver atoms are represented respectively in magenta, red, cyan and gray. When moving on the H$_2$O covered surface (f-j), the silver atom is always attached to a water molecule. This Ag-H$_2$O bond has the double effect of flattening the PES and preventing the repulsive interaction between Ag and the surface Zn atoms.

CONCLUSIONS

In conclusion, we have experimentally and theoretically demonstrated the complex influence of moisture on ionic dynamics and electronic properties in a single crystalline ZnO NW memristive model system. Adsorbed moisture decreases the electronic conductivity due to the modification of electronic surface properties, but decreases the forming voltage and ensures reliable device operation due to the influence on nanoionic processes underlaying resistive switching effects. DFT calculations have shown that water molecules on the NW surfaces are responsible for a severe decrease of the diffusion barrier of Ag^+ ions along the NW axis, facilitating the conductive filament formation. These results revealed the dual nature of adsorbed water molecules from ambient, playing a fundamental role in regulating the resistive switching mechanism.

ASSOCIATED CONTENT

Supporting Information. As-grown ZnO NWs; Effect of adsorbed species on electronic transport properties; Influence of moisture on electroforming – additional data; Direct observation of the effect of moisture on resistive switching; Reversibility of resistive switching behavior;

AUTHOR INFORMATION

Corresponding Authors

Ilia Valov: i.valov@fz-juelich.de;

Carlo Ricciardi: carlo.ricciardi@polito.it

‡G.M. and F.R. contributed equally to this work.

Notes

There are no conflicts of interest to declare.

REFERENCES

(1)   Ielmini, D.; Waser, R. *Resistive Switching - From Fundamentals of Nanoionic Redox Processes to Memristive Device Applications*; Wiley-VCH: Weinheim, 2016.

(2)   Jo, S. H.; Chang, T.; Ebong, I.; Bhadviya, B. B.; Mazumder, P.; Lu, W. Nanoscale Memristor Device as Synapse in Neuromorphic Systems. *Nano Lett.* **2010**, *10* (4), 1297–1301. https://doi.org/10.1021/nl904092h.

(3)   Wang, Z.; Joshi, S.; Savel'ev, S. E.; Jiang, H.; Midya, R.; Lin, P.; Hu, M.; Ge, N.; Strachan, J. P.; Li, Z.; Wu, Q., Barnell, M.; Li, G.L.; Xin, H.L.; Williams, R.S.; Xia, Q.; Yang, J.J. Memristors with Diffusive Dynamics as Synaptic Emulators for Neuromorphic Computing. *Nat. Mater.* **2017**, *16* (1), 101–108. https://doi.org/10.1038/nmat4756.

(4)   Milano, G.; Luebben, M.; Ma, Z.; Dunin-Borkowski, R.; Boarino, L.; Pirri, C. F.; Waser, R.; Ricciardi, C.; Valov, I. Self-Limited Single Nanowire Systems Combining All-in-One Memristive and Neuromorphic Functionalities. *Nat. Commun.* **2018**, *9* (1), 5151. https://doi.org/10.1038/s41467-018-07330-7.

(5)   Milano, G.; Pedretti, G.; Fretto, M.; Boarino, L.; Benfenati, F.; Ielmini, D.; Valov, I.; Ricciardi, C. Brain-Inspired Structural Plasticity through Reweighting and Rewiring in Multi-Terminal Self-Organizing Memristive Nanowire Networks. *Adv. Intell. Syst.* **2020**, 2000096. https://doi.org/10.1002/aisy.202000096.

(6)   Li, X.; Tang, J.; Zhang, Q.; Gao, B.; Yang, J. J.; Song, S.; Wu, W.; Zhang, W.; Yao, P.; Deng, N.; Deng., L.; Xie, Y.; Qian, H.; Wu, H.; Power-Efficient Neural Network with

Artificial Dendrites. *Nat. Nanotechnol.* **2020**. https://doi.org/10.1038/s41565-020-0722-5.

(7)   Wang, L.; Wang, Z.; Zhao, W.; Hu, B.; Xie, L.; Yi, M.; Ling, H.; Zhang, C.; Chen, Y.; Lin, J.; Zhu, J.; Huang, W. Controllable Multiple Depression in a Graphene Oxide Artificial Synapse. *Adv. Electron. Mater.* **2017**, *3* (1), 1600244. https://doi.org/10.1002/aelm.201600244.

(8)   Prezioso, M.; Merrikh-Bayat, F.; Hoskins, B. D.; Adam, G. C.; Likharev, K. K.; Strukov, D. B. Training and Operation of an Integrated Neuromorphic Network Based on Metal-Oxide Memristors. *Nature* **2015**, *521* (7550), 61–64. https://doi.org/10.1038/nature14441.

(9)   Wang, Z.; Joshi, S.; Savel'ev, S.; Song, W.; Midya, R.; Li, Y.; Rao, M.; Yan, P.; Asapu, S.; Zhuo, Y.; Jiang, H.; Lin, P.; Li, C.; Yoon, J.H.; Upadhyay, N.K.; Zhang, J.; Hu, M.; Strachan, J.P.; Barnell, M.; Wu, Q.; Wu, H., Williams, R.S.; Xia, Q.; Yang, J.J. Fully Memristive Neural Networks for Pattern Classification with Unsupervised Learning. *Nat. Electron.* **2018**, *1* (2), 137–145. https://doi.org/10.1038/s41928-018-0023-2.

(10)   Li, C.; Wang, Z.; Rao, M.; Belkin, D.; Song, W.; Jiang, H.; Yan, P.; Li, Y.; Lin, P.; Hu, M.; Ge, N.; Strachan, J.P.; Barnell,M.; Wu, Q.; Williams, R.S.; Yang, J.J.; Xia, Q. Long Short-Term Memory Networks in Memristor Crossbar Arrays. *Nat. Mach. Intell.* **2019**, *1* (1), 49–57. https://doi.org/10.1038/s42256-018-0001-4.

(11)   Cai, F.; Correll, J. M.; Lee, S. H.; Lim, Y.; Bothra, V.; Zhang, Z.; Flynn, M. P.; Lu, W. D. A Fully Integrated Reprogrammable Memristor–CMOS System for Efficient Multiply–Accumulate Operations. *Nat. Electron.* **2019**, *2* (7), 290–299.

https://doi.org/10.1038/s41928-019-0270-x.

(12)   Cai, F.; Kumar, S.; Van Vaerenbergh, T.; Sheng, X.; Liu, R.; Li, C.; Liu, Z.; Foltin, M.; Yu, S.; Xia, Q.; Yang, J. J.; Beausoleil, R., Lu, W.D.; Strachan, J.P. Power-Efficient Combinatorial Optimization Using Intrinsic Noise in Memristor Hopfield Neural Networks. *Nat. Electron.* **2020**, *3* (7), 409–418. https://doi.org/10.1038/s41928-020-0436-6.

(13)   Strukov, D. B.; Snider, G. S.; Stewart, D. R.; Williams, R. S. The Missing Memristor Found. *Nature* **2008**, *453* (7191), 80–83. https://doi.org/10.1038/nature06932.

(14)   Yang, J. J.; Pickett, M. D.; Li, X.; Ohlberg, D. A. A.; Stewart, D. R.; Williams, R. S. Memristive Switching Mechanism for Metal/Oxide/Metal Nanodevices. *Nat. Nanotechnol.* **2008**, *3* (7), 429–433. https://doi.org/10.1038/nnano.2008.160.

(15)   Yang, J. J.; Strukov, D. B.; Stewart, D. R. Memristive Devices for Computing. *Nat. Nanotechnol.* **2013**, *8* (1), 13–24. https://doi.org/10.1038/nnano.2012.240.

(16)   Chen, J.-Y.; Wu, M.-C.; Ting, Y.-H.; Lee, W.-C.; Yeh, P.-H.; Wu, W.-W. Applications of P-n Homojunction ZnO Nanowires to One-Diode One-Memristor RRAM Arrays. *Scr. Mater.* **2020**, *187*, 439–444. https://doi.org/10.1016/j.scriptamat.2020.06.061.

(17)   Ismail, M.; Abbas, H.; Choi, C.; Kim, S. Stabilized and RESET-Voltage Controlled Multi-Level Switching Characteristics in ZrO2-Based Memristors by Inserting a-ZTO Interface Layer. *J. Alloys Compd.* **2020**, *835*, 155256. https://doi.org/10.1016/j.jallcom.2020.155256.

(18)   Waser, R.; Dittmann, R.; Staikov, G.; Szot, K. Redox-Based Resistive Switching Memories

- Nanoionic Mechanisms, Prospects, and Challenges. *Adv. Mater.* **2009**, *21* (25–26), 2632–2663. https://doi.org/10.1002/adma.200900375.

(19)   Valov, I.; Tsuruoka, T. Effects of Moisture and Redox Reactions in VCM and ECM Resistive Switching Memories. *J. Phys. D. Appl. Phys.* **2018**, *51* (41), 413001. https://doi.org/10.1088/1361-6463/aad581.

(20)   Tsuruoka, T.; Terabe, K.; Hasegawa, T.; Valov, I.; Waser, R.; Aono, M. Effects of Moisture on the Switching Characteristics of Oxide-Based, Gapless-Type Atomic Switches. *Adv. Funct. Mater.* **2012**, *22* (1), 70–77. https://doi.org/10.1002/adfm.201101846.

(21)   Tappertzhofen, S.; Valov, I.; Tsuruoka, T.; Hasegawa, T.; Waser, R.; Aono, M. Generic Relevance of Counter Charges for Cation-Based Nanoscale Resistive Switching Memories. *ACS Nano* **2013**, *7* (7), 6396–6402. https://doi.org/10.1021/nn4026614.

(22)   Tao, Y.; Wang, Z.; Xu, H.; Ding, W.; Zhao, X.; Lin, Y.; Liu, Y. Moisture-Powered Memristor with Interfacial Oxygen Migration for Power-Free Reading of Multiple Memory States. *Nano Energy* **2020**, 104628. https://doi.org/10.1016/j.nanoen.2020.104628.

(23)   Lübben, M.; Menzel, S.; Park, S. G.; Yang, M.; Waser, R.; Valov, I. SET Kinetics of Electrochemical Metallization Cells: Influence of Counter-Electrodes in SiO 2 /Ag Based Systems. *Nanotechnology* **2017**, *28* (13), 135205. https://doi.org/10.1088/1361-6528/aa5e59.

(24)   Lübben, M.; Wiefels, S.; Waser, R.; Valov, I. Processes and Effects of Oxygen and Moisture

in Resistively Switching TaO x and HfO X. *Adv. Electron. Mater.* **2018**, *4* (1), 1700458. https://doi.org/10.1002/aelm.201700458.

(25) Heisig, T.; Baeumer, C.; Gries, U. N.; Mueller, M. P.; La Torre, C.; Luebben, M.; Raab, N.; Du, H.; Menzel, S.; Mueller, D. N.; Jia, C.L. ; Mayer, J. ; Waser, R., Valov, I., De Souza, R.A., Dittmann, R. Oxygen Exchange Processes between Oxide Memristive Devices and Water Molecules. *Adv. Mater.* **2018**, *30* (29), 1800957. https://doi.org/10.1002/adma.201800957.

(26) Messerschmitt, F.; Kubicek, M.; Rupp, J. L. M. How Does Moisture Affect the Physical Property of Memristance for Anionic-Electronic Resistive Switching Memories? *Adv. Funct. Mater.* **2015**, *25* (32), 5117–5125. https://doi.org/10.1002/adfm.201501517.

(27) Messerschmitt, F.; Jansen, M.; Rupp, J. L. M. When Memristance Crosses the Path with Humidity Sensing—About the Importance of Protons and Its Opportunities in Valence Change Memristors. *Adv. Electron. Mater.* **2018**, *4* (12), 1800282. https://doi.org/10.1002/aelm.201800282.

(28) Valov, I.; Linn, E.; Tappertzhofen, S.; Schmelzer, S.; van den Hurk, J.; Lentz, F.; Waser, R. Nanobatteries in Redox-Based Resistive Switches Require Extension of Memristor Theory. *Nat. Commun.* **2013**, *4* (1), 1771. https://doi.org/10.1038/ncomms2784.

(29) Lübben, M.; Karakolis, P.; Ioannou-Sougleridis, V.; Normand, P.; Dimitrakis, P.; Valov, I. Graphene-Modified Interface Controls Transition from VCM to ECM Switching Modes in Ta/TaO x Based Memristive Devices. *Adv. Mater.* **2015**, *27* (40), 6202–6207.

https://doi.org/10.1002/adma.201502574.

(30)   Xiao, B.; Watanabe, S. Moisture Effect on the Diffusion of Cu Ions in Cu/Ta 2 O 5 /Pt and

Cu/SiO 2 /Pt Resistance Switches: A First-Principles Study. *Sci. Technol. Adv. Mater.* **2019**,

20 (1), 580–588. https://doi.org/10.1080/14686996.2019.1616222.

(31)   Tsuruoka, T.; Valov, I.; Tappertzhofen, S.; van den Hurk, J.; Hasegawa, T.; Waser, R.;

Aono, M. Redox Reactions at Cu,Ag/Ta 2 O 5 Interfaces and the Effects of Ta 2 O 5 Film

Density on the Forming Process in Atomic Switch Structures. *Adv. Funct. Mater.* **2015**, *25*

(40), 6374–6381. https://doi.org/10.1002/adfm.201500853.

(32)   Chang, C.; Chen, J.; Huang, C.; Chiu, C.; Lin, T.; Yeh, P.-H.; Wu, W.-W. Direct

Observation of Dual-Filament Switching Behaviors in Ta 2 O 5 -Based Memristors. *Small*

2017, *13* (15), 1603116. https://doi.org/10.1002/smll.201603116.

(33)   Nagashima, K.; Yanagida, T.; Oka, K.; Kanai, M.; Klamchuen, A.; Kim, J.-S; Park, B. H.;

Kawai, T. Intrinsic Mechanisms of Memristive Switching. *Nano Lett.* **2011**, *11* (5), 2114–

2118. https://doi.org/10.1021/nl200707n.

(34)   Nagashima, K.; Yanagida, T.; Oka, K.; Kanai, M.; Klamchuen, A.; Rahong, S.; Meng, G.;

Horprathum, M.; Xu, B.; Zhuge, F.; He, Y.; Park H.B.; Kawai T.; Prominent

Thermodynamical Interaction with Surroundings on Nanoscale Memristive Switching of

Metal Oxides. *Nano Lett.* **2012**, *12* (11), 5684–5690. https://doi.org/10.1021/nl302880a.

(35)   Milano, G.; Porro, S.; Valov, I.; Ricciardi, C. Recent Developments and Perspectives for

Memristive Devices Based on Metal Oxide Nanowires. *Adv. Electron. Mater.* **2019**, *5* (9), 1800909. https://doi.org/10.1002/aelm.201800909.

(36)   Porro, S.; Risplendi, F.; Cicero, G.; Bejtka, K.; Milano, G.; Rivolo, P.; Jasmin, A.; Chiolerio, A.; Pirri, C. F.; Ricciardi, C. Multiple Resistive Switching in Core–Shell ZnO Nanowires Exhibiting Tunable Surface States. *J. Mater. Chem. C* **2017**, *5* (40), 10517–10523. https://doi.org/10.1039/C7TC02383A.

(37)   Milano, G.; Porro, S.; Ali, M. Y.; Bejtka, K.; Bianco, S.; Beccaria, F.; Chiolerio, A.; Pirri, C. F.; Ricciardi, C. Unravelling Resistive Switching Mechanism in ZnO NW Arrays: The Role of the Polycrystalline Base Layer. *J. Phys. Chem. C* **2018**, *122* (1), 866–874. https://doi.org/10.1021/acs.jpcc.7b09978.

(38)   Milano, G.; Boarino, L.; Ricciardi, C. Junction Properties of Single ZnO Nanowires with Asymmetrical Pt and Cu Contacts. *Nanotechnology* **2019**, *30* (24), 244001. https://doi.org/10.1088/1361-6528/ab0a9c.

(39)   Milano, G.; D'Ortenzi, L.; Bejtka, K.; Mandrile, L.; Giovannozzi, A. M.; Boarino, L.; Pirri, C. F.; Ricciardi, C.; Porro, S. Tuning ZnO Nanowire Dissolution by Electron Beam Modification of Surface Wetting Properties. *J. Phys. Chem. C* **2018**, *122* (14), 8011–8021. https://doi.org/10.1021/acs.jpcc.8b01158.

(40)   Giannozzi, P.; Baroni, S.; Bonini, N.; Calandra, M.; Car, R.; Cavazzoni, C.; Ceresoli, D.; Chiarotti, G. L.; Cococcioni, M.; Dabo, I.; Dal Corso A.; de Gironcoli, S.; Fabris, S.; Fratesi, G.; Gabauer, R.; Gerstmann, U.; Gougoussis, C.; Kokalj, A.; Lazzeri, M.; Martin-Samos,

L.; Marzari, N.; Mauri, F.; Mazzarello, R.; Paolini, S.; Pasquarello, A.; Paulatto, L.; Sbraccia, C.; Scandolo, S.; Sclauzero, G.; Seitsonen, A. P; Smogunov, A.; Umari, P.; Wentzcovitch, R.M.. QUANTUM ESPRESSO: A Modular and Open-Source Software Project for Quantum Simulations of Materials. *J. Phys. Condens. Matter* **2009**, *21* (39), 395502. https://doi.org/10.1088/0953-8984/21/39/395502.

(41)   Perdew, J. P.; Burke, K.; Ernzerhof, M. Generalized Gradient Approximation Made Simple. *Phys. Rev. Lett.* **1996**, *77* (18), 3865–3868. https://doi.org/10.1103/PhysRevLett.77.3865.

(42)   Vanderbilt, D. Soft Self-Consistent Pseudopotentials in a Generalized Eigenvalue Formalism. *Phys. Rev. B* **1990**, *41* (11), 7892–7895. https://doi.org/10.1103/PhysRevB.41.7892.

(43)   Miranda, E.; Milano, G.; Ricciardi, C. Modeling of Short-Term Synaptic Plasticity Effects in ZnO Nanowire-Based Memristors Using a Potentiation-Depression Rate Balance Equation. *IEEE Trans. Nanotechnol.* **2020**, *19*, 609–612. https://doi.org/10.1109/TNANO.2020.3009734.

(44)   Miranda, E.; Milano, G.; Ricciardi, C. Compact Modeling of the I-V Characteristics of ZnO Nanowires Including Nonlinear Series Resistance Effects. *IEEE Trans. Nanotechnol.* **2020**, 1–1. https://doi.org/10.1109/TNANO.2020.2981214.

(45)   Milano, G.; Luebben, M.; Laurenti, M.; Porro, S.; Bejtka, K.; Bianco, S.; Breuer, U.; Boarino, L.; Valov, I.; Ricciardi, C. Ionic Modulation of Electrical Conductivity of ZnO Due to Ambient Moisture. *Adv. Mater. Interfaces* **2019**, *6* (17), 1900803.

https://doi.org/10.1002/admi.201900803.

(46)   Li, Z.; Yang, R.; Yu, M.; Bai, F.; Li, C.; Wang, Z. L. Cellular Level Biocompatibility and Biosafety of ZnO Nanowires. *J. Phys. Chem. C* **2008**, *112* (51), 20114–20117. https://doi.org/10.1021/jp808878p.

(47)   Qi, J.; Huang, J.; Paul, D.; Ren, J.; Chu, S.; Liu, J. Current Self-Complianced and Self-Rectifying Resistive Switching in Ag-Electroded Single Na-Doped ZnO Nanowires. *Nanoscale* **2013**, *5* (7), 2651. https://doi.org/10.1039/c3nr00027c.

(48)   Wang, B.; Ren, T.; Chen, S.; Zhang, B.; Zhang, R.; Qi, J.; Chu, S.; Huang, J.; Liu, J. Resistive Switching in Ga- and Sb-Doped ZnO Single Nanowire Devices. *J. Mater. Chem. C* **2015**, *3* (45), 11881–11885. https://doi.org/10.1039/C5TC02102B.

(49)   Raffone, F.; Risplendi, F.; Cicero, G. A New Theoretical Insight Into ZnO NWs Memristive Behavior. *Nano Lett.* **2016**, *16* (4), 2543–2547. https://doi.org/10.1021/acs.nanolett.6b00085.

(50)   Yang, Y.; Gao, P.; Gaba, S.; Chang, T.; Pan, X.; Lu, W. Observation of Conducting Filament Growth in Nanoscale Resistive Memories. *Nat. Commun.* **2012**, *3* (1), 732. https://doi.org/10.1038/ncomms1737.

(51)   Yang, Y.; Gao, P.; Li, L.; Pan, X.; Tappertzhofen, S.; Choi, S.; Waser, R.; Valov, I.; Lu, W. D. Electrochemical Dynamics of Nanoscale Metallic Inclusions in Dielectrics. *Nat. Commun.* **2014**, *5* (1), 4232. https://doi.org/10.1038/ncomms5232.

(52) Zhou, J.; Xu, N. S.; Wang, Z. L. Dissolving Behavior and Stability of ZnO Wires in Biofluids: A Study on Biodegradability and Biocompatibility of ZnO Nanostructures. *Adv. Mater.* **2006**, *18* (18), 2432–2435. https://doi.org/10.1002/adma.200600200.

(53) Kenmoe, S.; Biedermann, P. U. Water Aggregation and Dissociation on the ZnO(10$\bar{1}$0) Surface. *Phys. Chem. Chem. Phys.* **2017**, *19* (2), 1466–1486. https://doi.org/10.1039/C6CP07516A.

(54) Raffone, F.; Cicero, G. Does Platinum Play a Role in the Resistance Switching of ZnO Nanowire-Based Devices? *Solid State Ionics* **2017**, *299*, 93–95. https://doi.org/10.1016/j.ssi.2016.10.020.

TABLE OF CONTENTS (TOC) GRAPHIC